Original scientific paper
https://doi.org/10.33180/InfMIDEM2018.409

Informacije MIDEM
Journal of Microelectronics,
Electronic Components and Materials
Vol. 48, No. 4(2018), 255 – 261

Multiparameter miniature fiber-optic sensor: design and signal interrogation

Simon Pevec[1], Borut Lenardič[2], Denis Đonlagić[1]

[1]University of Maribor, Faculty of EE & Computer Science, Maribor, Slovenia
[2]Optacore d.o.o., Ljubljana, Ljubljana, Slovenia

Abstract: Miniature, all-silica, fiber-optic sensors capable of independent measurement of at least two different parameters are presented. Sensors were produced by a micromachining process based on the selective etching of specially designed phosphorous-doped optical fibers and an assembly-procedure that included fiber cleaving, fiber splicing and etching of fiber-micro-assemblies. Furthermore, an efficient method for independent readout of parameters in sensors that are composed of multiple resonators was also developed. The method utilizes a discrete Furrier transform of sensor's optical spectrum and allows for simultaneous, crosstalk-free and highly sensitive readout of individual resonators' path length changes.

Keywords: Optical sensors; micromachinin; microstructures; discrete Fourier transform.

Večparametrični miniaturni optični vlakenski senzorji: načrtovanje in signalno razločevanje

Izvleček: V članku so predstavljeni miniaturni, optični, vlakenski senzorji, ki lahko neodvisno zaznavajo najmanj dva različna parametra. Senzorji so izdelani s postopkom mikroobdelave na osnovi selektivnega jedkanja posebnih z fosforjem dopiranih optičnih vlaken. Ti postopki so združeni s standardnimi postopki rezanja, varjenja in jedkanja. Poleg tega je predstavljena učinkovita metoda za neodvisno branje parametrov senzorja, ki združuje več zaporedno nanizanih resonatorjev. Metoda vključuje diskretno Fourierjevo transformacijo optičnega spektra, ki omogoča simultano in zelo občutljivo razločevanje sprememb posameznih optičnih dolžin resonatorjev.

Ključne besede: Optični senzorji; mikroobdelava; mikrostrukture; diskretna Fourierjeva transformacija.

** Corresponding Author's e-mail: simon.pevec@um.si*

1 Introduction

Optical fiber-based sensors have received a great deal of attention over the past several decades for increased sensitivity over existing techniques, geometric versatility, immunity to harsh environments, and inherent compatibility with optical fiber communication systems. The rising complexity of sensor systems, methods often require sensing of more than one physical or chemical parameter. In particular, multi-parameter fiber-optic sensors that monitor physical, chemical, and biological parameters are of great importance in numerous areas including structural health monitoring, environmental pollution control, biochemical and biomedical applications [1-4]. Miniaturization brings additional challenges in cases of small sensing devices designs, as those devices are more sensitive to oxidation and other degradation processes. A variety of multi-parameter sensors have been proposed recently including Fiber Bragg grating [5], Fabry-Perot interferometer (*FPI*) [6], higher-order-mode fiber based modal interferometer sensors [7], evanescent field sensors [8], surface plasmon resonance sensors [9] and combination between them [10]. Beside them, there are also some other techniques involving multicore fibers, that have high potential for multiparameter sensing [11].

In this paper we present all-silica multiparameter miniature fiber-optic Fabry-Perot (*FP*) sensors for measuring at least two parameters simultaneously. Sensor design, signal interrogation and achieved performance is presented and discussed for following multiparameter sensors:

- sensor for pressure and temperature [12]
- sensor for pressure and refractive index [13]

- sensor for refractive index and temperature [14]
- sensor for relative humidity and temperature [15]
- sensor for pressure, temperature, thermal conductivity and refractive index [16]

All sensors demonstrated high measurement resolution with negligible cross-talk among measured parameters. We successfully demonstrated simultaneous measurement up to four very different physical parameters. In addition, efficient method for independent readout of different parameters of multiple resonators was also presented. The method base on discrete Furrier transform of sensor's back reflected optical spectrum that allows simultaneous, crostallk-free and highly sensitive measurements of resonators' path length change.

2 Mathematical model and signal processing of fabry-perot multiparameter sensor

The model of the multiparameter sensor, which was used in simulations to illustrate the cross-talk between different frequency components and effect of applied Gaussian window, will be presented below.

Sensor is composed from three semi reflective surfaces, which forms three *FP* resonators. The first two are shown in the Fig.1 as L_1 and L_2, while the third resonator L_3 represents their sum. The basic principle of the operation of an individual *FP* resonator or interferometer can be explained by the light wave that enters the resonator, where it is reflected or interfered between the two surfaces. The magnitude of the light current or the shape of the spectral characteristic is effected by: the distance *L* between mirrors, the wavelength of light *λ* and the refractive index *n* of the transmission medium. Because in our case we have several *FP* resonators in the series, we can use one-dimensional space, where the superposition of the optical wave can be presented with a trigonometric approach.

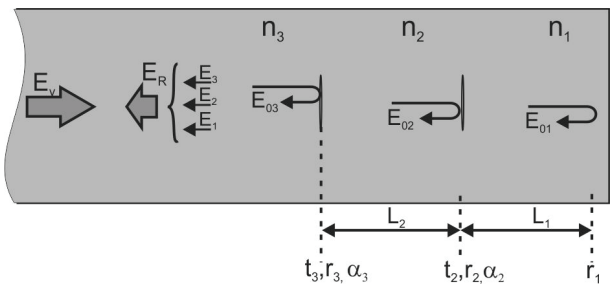

Figure 1: Model of FPI.

In general, the optical wavelength in some point can be described as a function of time:

$$E = E_0 \sin(\omega t \pm \varphi) \tag{1}$$

This can be written in the complex space as:

$$E = E_0 e^{j(\omega t \pm \varphi)} \tag{2}$$

First, three waves overlapping in space of the same frequency and speed must be add together.

The following waves are summed up after the reflection from the mirrors in the lead-in fiber:

$$\begin{aligned} E_{03} &= E_V r_3 \cdot e^{j\omega t} \\ E_{02} &= E_V t_3 r_2 \sqrt{1-\alpha_3} \cdot e^{j(\omega t+\varphi_1)} \\ E_{01} &= E_V t_3 t_2 r_1 \sqrt{1-\alpha_3}\sqrt{1-\alpha_2} \cdot e^{j(\omega t+\varphi_2)} \end{aligned} \tag{3}$$

Where E_{03}, E_{02}, and E_{01} are individual components of the electrical field strength, that are reflected from individual semi-reflective surfaces, *Ev* is the input amplitude of the electric field strength, r is coefficient of reflectivity and *t* is transmission coefficient, and the coefficient *α* is reserved for describing the optical losses on the splice.

The phase changes corresponded to the interferometer's optical path length variations: φ=kn=2πLn/λ, in our case, we have already defined it as a phase change due to a reflection from a distant mirror, which doubling the optical path, and thus the phase of the wave.

$$\begin{aligned} \varphi_1 &= \frac{4\pi n_2 L_2}{\lambda} \\ \varphi_2 &= \frac{4\pi\left(n_2 L_2 + n_1 L_1\right)}{\lambda} + \pi \end{aligned} \tag{4}$$

When optical waves travels cross the glass / air boundary, or vice versa, an additional phase shift occurs for *π* / 2, so in our example, when we observe the reflected wave, this is taken into account with the phase delay *π* (equation 4).

The current description covers only electric field strengths that do not include transmission coefficients t of individual mirrors on the way back. This is supplemented by the following terms:

$$\begin{aligned} E_3 &= E_{03} = E_v r_3 \cdot e^{j\omega t} \\ E_2 &= E_{02} t_3 \sqrt{1-\alpha_3} = E_v t_3^2 r_2 (1-\alpha_3) \cdot e^{j(\omega t+\varphi_1)} \\ E_1 &= E_{01} t_3 t_2 \sqrt{1-\alpha_3}\sqrt{1-\alpha_2} = \\ &= E_v t_3^2 t_2^2 r_1 (1-\alpha_3)(1-\alpha_2) \cdot e^{j(\omega t+\varphi_2)} \end{aligned} \tag{5}$$

Where E_3, E_2 and E_1 represent the total electrical field strength, which is reflected from the individual semi-reflective mirror, as shown in Fig. 1. Furthermore, the total electrical field strength can be written as the sum of all three components:

$$\begin{aligned} E_R &= E_3 + E_2 + E_1 \\ E_R &= E_v r_3 \cdot e^{j\omega t} + E_v t_3^2 r_2 (1-\alpha_3) \cdot e^{j(\omega t+\varphi_1)} + \\ &\quad + E_v t_3^2 t_2^2 r_1 (1-\alpha_3)(1-\alpha_2) \cdot e^{j(\omega t+\varphi_2)} \end{aligned} \tag{6}$$

Since the reflected-light intensity I_R is proportional to the square of the electric field strength, the following can be written as:

$$I_R \propto {E_R}^2 \tag{7}$$

When squaring, the conjugated complex value of the electric field strength must be taken into account:

$$\begin{aligned} I_R &\propto E_R E_R^* \\ I_R &\propto \left[\begin{array}{l} E_v r_3 \cdot e^{j\omega t} + E_v t_3^2 r_2 (1-\alpha_3) \cdot e^{j(\omega t+\varphi_1)} + \\ \quad + E_v t_3^2 t_2^2 r_1 (1-\alpha_3)(1-\alpha_2) \cdot e^{j(\omega t+\varphi_2)} \end{array} \right] \\ &\quad \cdot \left[\begin{array}{l} E_v r_3 \cdot e^{-j\omega t} + E_v t_3^2 r_2 (1-\alpha_3) \cdot e^{-j(\omega t+\varphi_1)} + \\ \quad + E_v t_3^2 t_2^2 r_1 (1-\alpha_3)(1-\alpha_2) \cdot e^{-j(\omega t+\varphi_2)} \end{array} \right] \end{aligned} \tag{8}$$

For more understandable presentation, the product will be written by combining individual coefficients into groups:

$$I_R \propto {E_V}^2 \left(\begin{array}{l} A + B\left(e^{-j\varphi_1} + e^{+j\varphi_1}\right) + \\ +C\left(e^{-j\varphi_2} + e^{+j\varphi_2}\right) + D\left(e^{-j(\varphi_2-\varphi_1)} + e^{+j(\varphi_2-\varphi_1)}\right) \end{array} \right) \tag{9}$$

$$\begin{aligned} A &= r_3^2 + r_2^2 t_3^4 (1-\alpha_3)^2 + r_1^2 t_3^4 t_2^4 (1-\alpha_3)^2 (1-\alpha_2)^2 \\ B &= r_3 r_2 t_3^2 (1-\alpha_3) \\ C &= r_3 r_1 t_3^2 t_2^2 (1-\alpha_3)(1-\alpha_2) \\ D &= r_2 r_1 t_3^4 t_2^2 (1-\alpha_3)^2 (1-\alpha_2) \end{aligned} \tag{10}$$

Taking into account the Euler's equation $e^{\pm jx} = \cos x \pm j \sin x$, we obtain:

$$I_R \propto {E_R}^2 \left[A + 2B\cos\varphi_1 + 2C\cos\varphi_2 + 2D\cos(\varphi_2 - \varphi_1) \right] \tag{11}$$

Since we calculate the reflected-light intensity, the reflective and transmission coefficients can be replaced by the reflectance R and the transmission T:

$$R = r^2, \quad T = t^2 \tag{12}$$

To reduce the set of unknowns of equations (4.11), by applying the law R + T = 1, the transmission can be replaced by the reflection and the group of coefficients can be written as follows:

$$\begin{aligned} A &= R_3 + R_2 (1-R_3)^2 (1-\alpha_3)^2 + \\ &\quad + R_1 (1-R_3)^2 (1-R_2)^2 (1-\alpha_3)^2 (1-\alpha_2)^2 \\ B &= \sqrt{R_3 R_2} (1-R_3)(1-\alpha_3) \\ C &= \sqrt{R_3 R_1} (1-R_3)(1-R_2)(1-\alpha_3)(1-\alpha_2) \\ D &= \sqrt{R_2 R_1} (1-R_3)^2 (1-R_2)(1-\alpha_3)^2 (1-\alpha_2) \end{aligned} \tag{13}$$

If we take into account the individual values of the phase angles and the fact that the reflected light intensity depends on the input light intensity, the final equation can be written as:

$$I_R = I_V \left[\begin{array}{l} A + 2B\cos\dfrac{4\pi n_2 L_2}{\lambda} + \\ \quad + 2C\cos\left(\dfrac{4\pi\left(n_2 L_2 + n_1 L_1\right)}{\lambda} + \pi \right) + \\ \quad + 2D\cos\left(\dfrac{4\pi n_1 L_1}{\lambda} + \pi \right) \end{array} \right] \tag{13}$$

We have shown that the total reflected-light intensity I_R of *FPI* with three semi-reflective surfaces can be described as a linear superposition of three cosine spectral components with distinctive spectral frequencies, which are determined by the length of the resonator, the refractive index (*RI*) of the transmission medium and the wavelength of light.

Further presented interrogation method involve straightforward solution for independent readout of individual *FP* resonators path length variations. Method based on discrete Furrier transform (*DFT*) of sensor's optical spectrum followed by phase tracking of corresponded frequency component. Basic definition of *DFT* is:

$$X_k = \sum_{n=0}^{N-1} x_n e^{-j\frac{2\pi}{N}nk}, \quad \mathrm{k} \in \{0,1,...,N-1\} \tag{14}$$

Where X_k is Fourier transform at k-th frequency component, N is the number of samples, and x_n is the n-th sample, which is then multiplied by a complex matrix of real and imaginary values. The method is especially useful because it enables us to calculate a complex matrix in advance, which depends only on the number of input samples. If we are interested only in changing the phase of a predefined frequency component, it is sufficient to calculate only the k-th component of the complex matrix, which additionally saves the processor time. When multiplying the input data with the k-th component, we obtain a complex number x+jy from which the value of the phase is calculated:

$$\varphi = \arctan\frac{\mathrm{Im}}{\mathrm{Re}} = \arctan\frac{y}{x} \tag{15}$$

The spectral characteristic in the wavelength space does not have a pure cosine characteristic, as the distance between the adjacent peaks is not constant regarding wavelength axis. To get a clean periodic cosine characteristic, the wavelength should be replaced by frequency taking into account basic law $\lambda=c/f$, where c presents speed of light in vacuum and f frequency. The mathematical model from equation (13) is transformed into the following form in the frequency domain:

$$I_R = I_V\left[\begin{array}{l} A+2B\cos\dfrac{4\pi n_2 L_2 f}{c}+ \\ \quad +2C\cos\left(\dfrac{4\pi\left(n_2L_2+n_1L_1\right)f}{c}+\pi\right)+ \\ \quad +2D\cos\left(\dfrac{4\pi n_1 L_1 f}{c}+\pi\right) \end{array}\right] \tag{16}$$

To show significance of frequency domain and of applying a Gaussian window, we simulated dual cavity *FPI*, calculate *DFT* in wavelength and frequency domain, once with and once without Gaussian window. One example of simulated spectrum is shown on Fig.2.

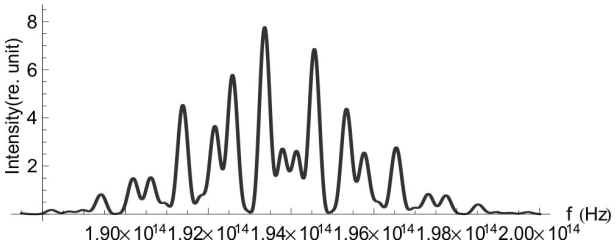

Figure 2: Typical back-reflected spectrum of dual FPI (L_1=100 μm, L_2=160 μm, n=1.45) with applied Gaussian window.

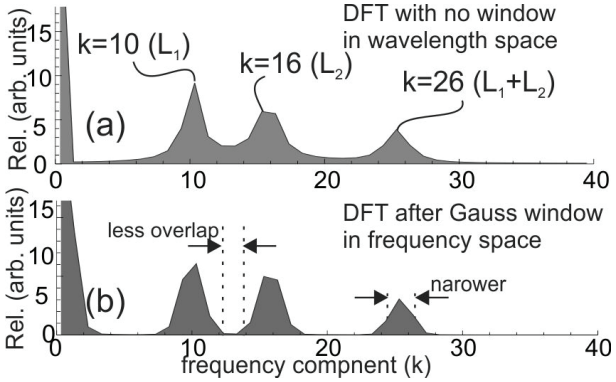

Figure 3: Simulated *FP* sensor with dual cavity length L_1=100 μm, L_2=160 μm, n=1.45, wavelength sweep was from 1510 to 1590 nm: (a) *DFT* in wavelength space with no applied window, (b) *DFT* in frequency space with Gaussian window.

The simulation results show that *DFT* in frequency domain with Gaussian window helps to isolate the individual frequency component to minimize crosstalk between them. The crosstalk between both components was reduced from few degrees to less than ±0.01 degree, when varying L_1 and observing phase change of L_2.

3 Multiparameter fiber optic sensors

Multiparameter fiber optic sensors are created by using micromachining technique based on selective etching [17]. Selective etching is a highly effective tool for realization of various optical sensors and microdevices. In general, the creation of a microdevice

based on selective-etching requires the design and manufacturing of a specially doped structure forming fiber (*SFF*). A short section of *SFF* is then spliced at the tip or in-between the lead-in single mode fibers (*SMF*) and then etched into the final structure. The tip of the *SFF* can also be directly etched into the desired microphotonic structure when the *SFF* incorporates a waveguide structure.

One example produced by selective etching is shown in Fig. 4.

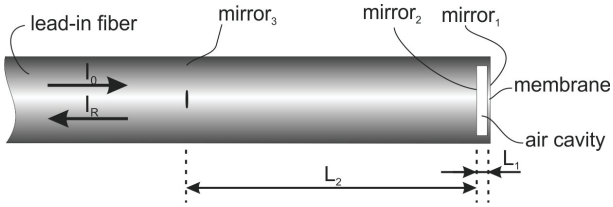

Figure 4: Dual parameter pressure-temperature sensor.

The sensor's design utilized dual all-fiber *FP* resonators with distinctive lengths that permitted straightforward spectrally-resolved interrogation of the sensor [12]. First shorter pressure sensitive *FP* resonator (L_1) is located on the fiber tip and consists of thin silica membrane and inner reflective surface. Temperature is measured by observing the optical path length change of the second *FP* resonator (L_2), which is mainly temperature dependent due to the silica's *RI* dependence on the temperature (i.e. *dn/dT* of silica corresponds to about 10^{-5} K^{-1}) Temperature measurements with all-silica structure positioned between two reflective surfaces is involved almost at all further presented sensors.

The temperature and pressure were efficiently and unambiguously determined by signal processing of the reflected optical-spectra. Reflected optical spectra of typical sensor is presented in Fig. 5.

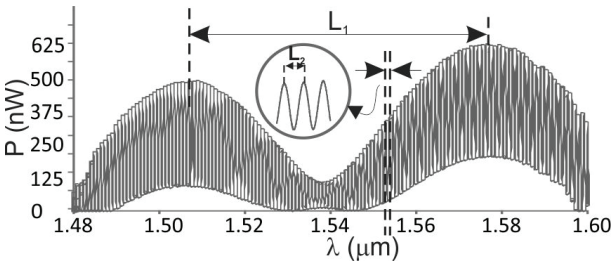

Figure 5: Output spectral characteristic of temperature pressure sensor (L_1=17 μm, L_2=1000 μm).

The sensor can be easily modified to cover different pressure and temperature ranges. In particular, its all-silica design and miniature size provides potential opportunities for its usage in high-temperature, biomedical and micro-fluidic systems.

Another example of multiparameter sensor is shown in Fig. 6, and present a miniature, all-silica, dual-parameter *FP* sensor for simultaneous measurement of surrounding fluid's *RI* and temperature [14]. Sensor consists of two stacked *FPI*, first *FPI* is U-shaped microcell for *RI* change measurements and second *FPI* is temperature sensitive segment. This sensor permits a full temperature-compensated high resolution *RI* measurement in range of 10^{-7} refractive index unit (*RIU*) as is shown on Fig. 7. High resolution measurement can be used to determine very small changes in fluid structure or composition. All-silica design provides high chemical and thermal inertness, while the miniature size provides opportunities for measuring very small (*nL*) fluid volumes.

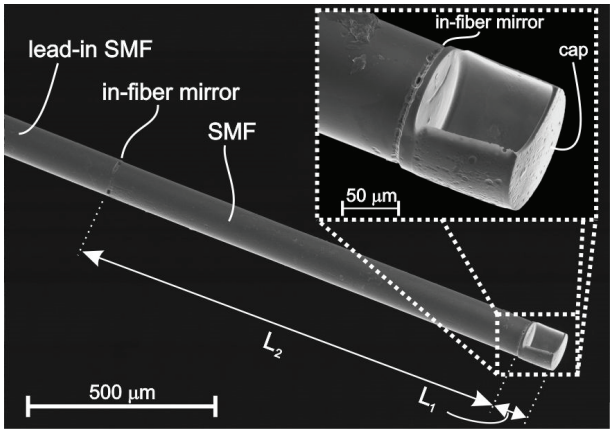

Figure 6: Dual parameter RI-temperature sensor.

Next example in Fig. 8 shows one more complex multiparameter *FP* sensor for simultaneous measurement of pressure and refractive index [13]. Sensor consists of microcell that allows surrounding fluid to freely enter inside to provide the detection of fluid's *RI* through the measurement of the microcell's optical path length.

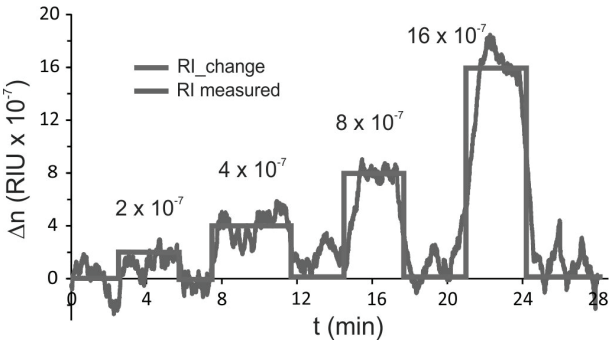

Figure 7: Demonstration of system RI resolution under varying temperature conditions.

Pressure measurements is realized by *FPI* created between thin silica diaphragm and inner reflective surface.

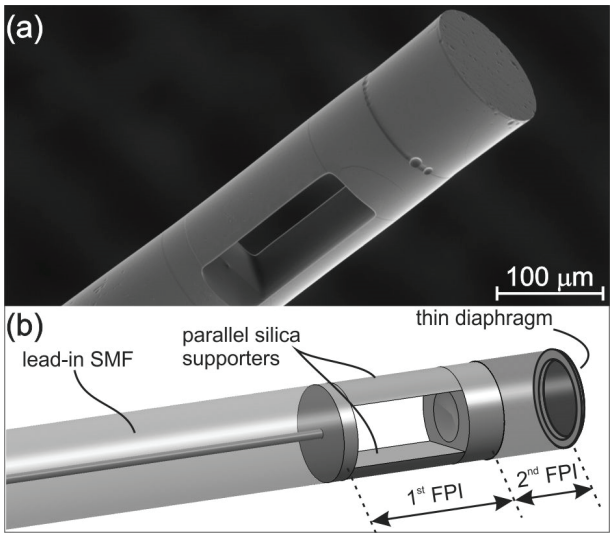

Figure 8: Pressure-refractive index sensor, (a) SEM photo, (b) proposed sensor design.

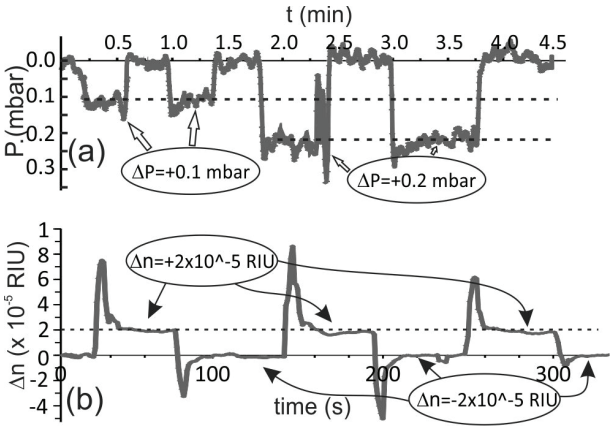

Figure 9: Sensor's response to P and *RI* change: (a) pressure resolution demonstration, (b) *RI* resolution demonstration.

High measurement resolutions better than 0.1 *mBar* and 2x10^{-5} *RIU* can be achieved by using spectral interrogation and a *DFT*-based measurement algorithm.

Another example of multiparameter sensor is shown in Fig. 10, and present a miniature, all-silica, dual-parameter *FP* sensor for simultaneous measurement of relative humidity (*RH*) and temperature [15].

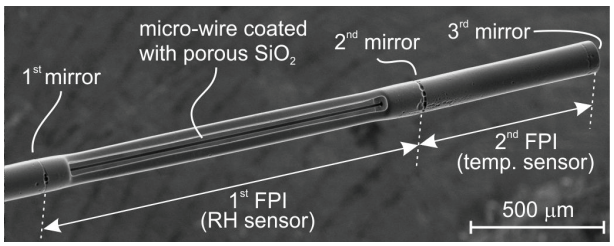

Figure 10: SEM image of RH sensor.

The sensor is composed of two cascaded *FPI*. The first *FPI* consists of a short silica micro-wire (diameter is cca. 13 μm) "sandwiched" in-between two semi-reflective in-fiber mirrors (mirrors 1 and 2 in Fig. 10).

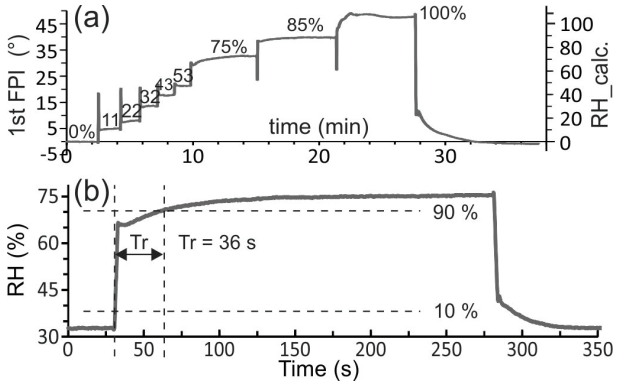

Figure 11: (a) Response of produced sensor to humidity change using about a 600 *nm* thick porous SiO_2 layer, (b) Dynamic response of *RH* sensor.

Micro-wire is coated by a thin layer of porous silica, and forms a *RH* sensing part. The second *FPI* consists of section created on the sensor tip that forms a temperature measuring part. The typical total length of produced sensor is less than 2 mm, while diameter doesn't exceed 125 μm. The sensor has good dynamic performances and covers broad *RH* measuring range as shown in Fig. 11. Sensor has also linear characteristics for both measurement parameters with sensitivity of 0.48 degree/%RH and 3.7 degree/°C.

The last and the most complex device is multiparameter all-silica fiber optic sensor for simultaneous measurement of pressure, *RI*, temperature and thermal conductivity of gases [16]. It is one of the few truly fiber solutions that allows measuring more than three parameters simultaneously.

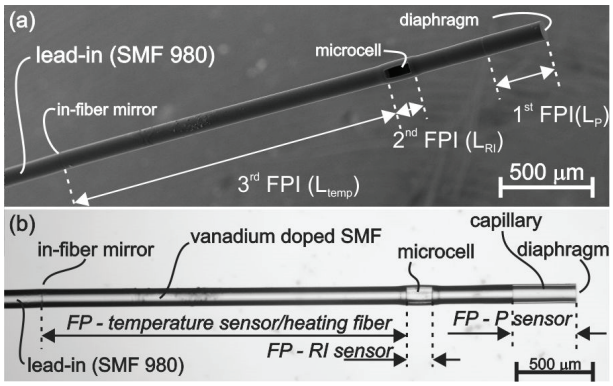

Figure 12: Fabricated multiparameter sensor: (a) *SEM* image; (b) optical microscope image.

The sensor utilizes three different *FPI* stacked on the tip of a lead-in optical fiber. The first *FPI* is made of a thin-wall glass capillary and thin silica diaphragm located on the top of the sensor structure. The *2nd FPI* is open path U-shaped all-silica microcell, which allows for free access of the surrounding gas in-between the *FPI's* semi-reflective surfaces and, thus, for gas *RI* measurements. A short section of Vanadium-Doped Fiber placed in between an in-fiber mirror and semi-reflective surface defines the *3rd FPI*. Vanadium doping induces high optical absorption at shorter wavelengths (i.e. 980 *nm*), while the increase in absorption near 1550 *nm* remains limited/low [18]. This *3rd FPI* performs two functions: Temperature sensing and thermal conductivity measurement. Temperature is measured by observing the optical path length change of the *3rd FPI*. On the other hand, the thermal conductivity is measured by application of active heating of this temperature sensitive segment.

Sensor has high repeatability and high resolutions of all four sensed parameters (a temperature resolution of 2 *mK*, pressure resolution of 1 *mbar*, *RI* resolution of 5x10^{-7} *RIU* and thermal conductivity of better than 1x10^{-3} *W/mK* were achieved).

4 Conclusions

This paper presented design and interrogation of many multiparameter Fabry-Perot sensors that are all capable of measuring at least two parameters simultaneously. Experimental results regarding crosstalk confirmed that independent and simultaneous readout of stacked *FP* resonators on the optical fiber is possible, which is consistent with simulated results obtained from a mathematical model.

In the future, sensors could be produced with even more *FP* resonators (more than 3), which is entirely feasible with this kind of micromachining technology and with this kind of signal interrogation, but it however increases the complexity of the sensor and hence also the price efficiency in compared to using multiple individual sensors.

5 Acknowledgments

We would like to thank the Slovenian Research Agency (ARRS) for supporting this work under Grant J2-8192 and P2-0368. We would also like to thank to Optacore d.o.o. for supplying the specialty fibers required for the sensor production.

6 References

1. P. Lutzow, D. Pergande, and H. Heidrich, "Integrated optical sensor platform for multiparameter biochemical analysis," Opt Express 19, 13277-13284 (2011). https://doi.org/10.1364/Oe.19.013277
2. Y. P. Xu, P. Lu, S. Gao, D. Xiang, P. Lu, S. Mihailov, and X. Y. Bao, "Optical fiber random grating-based multiparameter sensor," Opt Lett 40, 5514-5517 (2015). https://doi.org/10.1364/Ol.40.005514
3. V. Bhatia, "Applications of long-period gratings to single and multi-parameter sensing," Opt Express 4, 457-466 (1999). https://doi.org/Doi 10.1364/Oe.4.000457
4. Y. Chamorovskiy, "Specialty Optical Fibres for a Sensing Application," Inform Midem 40, 285-290 (2010).
5. H. Y. Meng, W. Shen, G. B. Zhang, C. H. Tan, and X. G. Huang, "Fiber Bragg grating-based fiber sensor for simultaneous measurement of refractive index and temperature," Sensor Actuat B-Chem 150, 226-229 (2010). https://doi.org/10.1016/j.snb.2010.07.010
6. S. Pevec and D. Donlagic, "Miniature fiber-optic Fabry-Perot refractive index sensor for gas sensing with a resolution of 5x10−9 RIU," Opt Express 26, 23868-23882 (2018). https://doi.org/10.1364/OE.26.023868
7. M. Boerkamp, Y. Y. Lu, J. Mink, Z. Zobenica, and R. W. van der Heijden, "Multiple Modes of a Photonic Crystal Cavity on a Fiber Tip for Multiple Parameter Sensing," J Lightwave Technol 33, 3901-3906 (2015). https://doi.org/10.1109/Jlt.2015.2448763
8. R. Biswas, "Low-cost wavelength-selective evanescent fiber optic temperature and refractive index sensor," Eur Phys J Plus 132(2017). https://doi.org/ARTN 207 10.1140/epjp/i2017-11509-6
9. W. Luo, S. Chen, L. Chen, H. L. Li, P. C. Miao, H. Y. Gao, Z. L. Hu, and M. Li, "Dual-angle technique for simultaneous measurement of refractive index and temperature based on a surface plasmon resonance sensor," Opt Express 25, 12733-12742 (2017). https://doi.org/10.1364/Oe.25.012733
10. M. M. Ali, M. R. Islam, K. S. Lim, D. S. Gunawardena, H. Z. Yang, and H. Ahmad, "PCF-Cavity FBG Fabry-Perot Resonator for Simultaneous Measurement of Pressure and Temperature," Ieee Sens J 15, 6921-6925 (2015). https://doi.org/10.1109/Jsen.2015.2468065
11. A. Samir and B. Batagelj, "A seven-core fibre for fluorescence spectroscopy," Inform Midem 47, 49-54 (2017).
12. S. Pevec and D. Donlagic, "Miniature all-fiber Fabry-Perot sensor for simultaneous measurement of pressure and temperature," Appl Optics 51, 4536-4541 (2012). https://doi.org/10.1364/Ao.51.004536
13. S. Pevec and D. Donlagic, "Miniature fiber-optic sensor for simultaneous measurement of pressure and refractive index," Opt Lett 39, 6221-6224 (2014). https://doi.org/10.1364/Ol.39.006221
14. S. Pevec and D. Donlagic, "High resolution, all-fiber, micro-machined sensor for simultaneous measurement of refractive index and temperature," Opt Express 22, 16241-16253 (2014). https://doi.org/10.1364/Oe.22.016241
15. S. Pevec and D. Donlagic, "Miniature all-silica fiber-optic sensor for simultaneous measurement of relative humidity and temperature," Opt Lett 40, 5646-5649 (2015). https://doi.org/10.1364/Ol.40.005646
16. S. Pevec and D. Donlagic, "MultiParameter Fiber-Optic Sensor for Simultaneous Measurement of Thermal Conductivity, Pressure, Refractive Index, and Temperature," Ieee Photonics J 9(2017). https://doi.org/10.1109/JPHOT.2017.2651978
17. S. Pevec, E. Cibula, B. Lenardic, and D. Donlagic, "Micromachining of optical fibers using the selective etching of doped silica glass," Micro-Optics 2012 8428(2012). https://doi.org/10.1117/12.922045
18. Z. Matjasec, S. Campelj, and D. Donlagic, "All-optical, thermo-optical path length modulation based on the vanadium-doped fibers," Opt Express 21, 11794-11807 (2013). https://doi.org/10.1364/Oe.21.011794

Arrived: 31. 08. 2018
Accepted: 09. 01. 2019